

Sparsity Dependent Metrics Depict Alteration of Brain Network Connectivity in Parkinson's Disease*

Tanmayee Samantaray, Jitender Saini and Cota Navin Gupta

Abstract— To date, regional brain atrophy unfolded using neuroimaging methods is observed to be the signature of Parkinson's disease (PD). In addition, graph theory-based studies are proving altered structural connectivity in PD. This motivated us to employ regional grey matter volume of PD patients (N=70) for comparative network analysis with an equal number of age- and gender-matched healthy controls (HC). In the current study, normalized grey matter maps obtained from structural magnetic resonance imaging (sMRI) were parcellated into 56 ROI (regions of interest) for construction of symmetric matrix using partial correlation between every pair of regional grey matter volumes. Sparsity thresholding was used to binarize the matrices and MATLAB functions from brain connectivity toolbox were employed to obtain the connectivity metrics. We observed PD with a significantly lower clustering coefficient as well as local efficiency at higher sparsities (above 0.9 and 0.84, respectively) with $p < 0.05$. The right fusiform gyrus was found to be the conserved hub, besides disruption of four hubs and regeneration of five other hubs. Lower clustering coefficient and local efficiency were indicative of reduced local integration and information processing, respectively. Hence, we suggest that global clustering coefficient and local efficiency could have a pivotal role in evaluating network topology. Thereby, our findings confirmed impairment of normal structural brain network topology reflecting disconnectivity mechanisms in PD.

Clinical Relevance— Analyzing structural brain connectivity in Parkinson's disease might provide the researchers and clinicians with a signature pattern of the disease to discriminate patients from normal controls.

I. INTRODUCTION

Parkinson's disease (PD), the second-most common neurodegenerative disorder, has been profoundly observed with major loss of dopaminergic neurons, and initiates at lower brainstem following to cortical regions [1]. Patients surviving with PD have both motor and non-motor symptoms, and due to unavailability of a proper curative might lead to fatal consequences. Although there is a lack of explicit clinical diagnostic scale and standard biomarker [2], [3] in PD, there is increasing evidence of studies associated with grey matter (GM) atrophy [4] and disconnectivity [5]–[9]. Of various available neuroimaging modalities, structural magnetic resonance imaging (sMRI) has successfully identified these regions and hence been used for exploring brain connectivity in our research.

In the current research work, we employed GM information for the construction of association matrix and

analyzed structural brain networks by deriving connectivity metrics at both local and global scales. The network features were obtained using MATLAB functions from Brain Connectivity Toolbox. We also performed comparative brain network analysis across a range of sparsity values.

II. MATERIALS AND METHODS

A. Participants

Seventy PD patients and an equal number of age- and gender-matched healthy controls (HC) were recruited at the Department of Neurology, National Institute of Mental Health and Neurosciences (NIMHANS), Bangalore, India. Signed and informed consent was provided by every patient and control. Demographic and clinical data of these subjects were also recorded. The clinical information and consent was in full compliance of NIMHANS Institutional Ethics Committee.

B. Data acquisition and Pre-processing of sMRI

The subjects were scanned using a 3T Philips Achieva scanner using a 32-channel head coil. The T1-weighted structural MRI were acquired using a magnetization prepared rapid acquisition gradient echo sequence (TR/TE: 8.2/3.7 ms, flip angle = 8, the field of view: 256 * 256 * 165 mm, 165 sagittal slices, voxel size = 1 * 1 * 1 mm). The raw images, obtained in DICOM format were converted into NIfTI format by MRICron's dcm2nii tool, available for download at <http://www.nitrc.org/projects/mricron>. These scans were pre-processed using Computational Anatomy Toolbox, CAT12 (<http://www.neuro.uni-jena.de/cat/>) within Statistical Parametric Mapping, SPM12 using MATLAB (Add version). These images were registered to the Montreal Neurological Institute (MNI) standard space tissue probability maps and segmented into different tissue types of which GM map was taken for further study.

C. Structural Network Construction

The grey matter maps of each group were parcellated based on LONI Probabilistic Brain Atlas, LPBA40 (<https://resource.loni.usc.edu/resources/atlasses-downloads/>) into 56 regions of interest (ROIs) as in Appendix, each ROI portraying a node in the network [10]. The regional grey matter volume (rGMV) of each of these 56 ROIs were obtained for each subject using CAT12, where volume implied the amount of tissue. Hence, for 70 HC subjects, we obtained the rGMV matrix of dimension 70*56. An

*T.S. was funded by Ministry of Human Resource Development (MHRD) doctoral scholarship by the Government of India. C.N.G.'s time was supported by Scheme for Promotion of Academic and Research Collaboration (SPARC Grant), Government of India, Project Code: P1073.

T.S. (corresponding author; +91- 361-258-2232; e-mail: tanma176106113@iitg.ac.in) and C.N.G. (e-mail: cngupta@iitg.ac.in) are with Neural Engineering Lab, Department of Biosciences and

Bioengineering, Indian Institute of Technology Guwahati, Guwahati, Assam 781039 India.

J.S. (e-mail: jsaini76@gmail.com) is with Department of Neuroimaging and Interventional Radiology, National Institute of Mental Health and Neurosciences, Bangalore, Karnataka 560030 India.

interregional association matrix of dimension 56*56 was constructed for each group based on partial correlation as number of subjects is greater than the number of regions [9], [11]. Prior to matrix construction, the effect of nuisance covariates such as age and gender were regressed out by performing a linear regression analysis. Any element of this association matrix, A_{ij} indicated the correlation between ROI i and j , removing the effect of other regions. These steps were coded in MATLAB (MathWorks R2020a).

D. Network metrics and analysis

The network matrix of each group was thresholded across a range of estimated sparsities for binarization to enable simplified network analysis [12]. Here, a sparsity threshold of 0.6 represented a matrix with the lowest 40% as zero, while considering the highest 60% values only. The network became almost equivalent to a random network (i.e. small-world index close to 1) below 0.6 sparsity, hence this value was selected as the lower limit for analysis [8], [12]. The average degree became less than the logarithm of number of nodes above sparsity of 0.9 at which small-world index is not estimable [8], [12]. The small-world network has equal number of nodes and edges as that of the network under study. In the current research study, random network contained 56 nodes and number of edges varied with sparsity with a maximum possible number of 1540 (i.e. $56*55/2$) edges, similar to that of the networks of our study. The small-world index (σ) is defined as having average shortest path length equivalent to that of random networks ($L_{study} \approx L_{rand}$) whereas clustering coefficient greater than that of random network ($C_{study} \gg C_{rand}$), where L_{study} and L_{rand} are the shortest path length of the network under study and random network respectively; and C_{study} and C_{rand} are the clustering coefficient of the network under study and random network respectively [13]. Hence, the range is optimized such that the network doesn't become extremely dense or extremely sparse, as extreme dense networks contain a lot of redundant edges, however, extreme sparse networks loose significant edges. Network measures viz., degree, mean clustering coefficient, mean local efficiency and betweenness centrality were calculated. Degree of a node is the number of edges it has to other nodes. Clustering coefficient of a node depicts the fraction of its neighbours connecting directly to each other; local efficiency of a node reveals how efficient the information transmits within its neighbours when it is removed [13]. Betweenness centrality of a node is a measure reflecting how densely it is connected in the entire network. These network metrics were estimated from Brain Connectivity Toolbox-derived functions [13]. Hubs are the regions with both degree and betweenness centrality one standard deviation higher than the respective mean [8]. The structural brain networks were visualized using BrainNet Viewer [14].

E. Statistical Analysis

A two-sample t-test was performed between PD and HC to investigate the age differences and a chi-square (χ^2) test for gender differences. A comparison at $P < 0.05$ was regarded as significant. A nonparametric permutation test [5] was conducted with 1000 repetitions, where the clustering

coefficients were randomly allocated to each of the groups in such a manner that the number of subjects in each randomized group remain the same as that of the original group. The randomized group differences in the network measures were then determined and used for permutation distribution of the difference. The actual between-group differences were then compared based on 95% confidence interval. The above steps were followed for group comparison of local efficiency as well. A self-written MATLAB code was developed in order to test the statistical significance of between-group differences in network metrics and perform comparative network analysis.

III. RESULTS AND DISCUSSIONS

A. Participants

No significant difference between PD patients and HC was found in age ($P = 0.077$) or gender ($P = 0.55$). The PD patients were observed with a mean Unified Parkinson's Disease Rating Scale (UPDRS) at off state at 30.09 ± 9.57 , mean UPDRS at on state at 17.50 ± 8.84 , mean age at onset of 47.74 ± 11.91 years, and median of H & Y score of 2 (Table 1).

TABLE 1. CHARACTERISTICS OF HEALTHY CONTROLS AND PARKINSON PATIENTS

Measures	Healthy Controls	Parkinson Patients	χ^2 / t-value	p-value
Count	70	70	-	-
Age in years (Mean \pm SD)	49.24 \pm 10.99	52.56 \pm 11.03	-1.78	0.0772
Age Range (years)	20-73	24-72	-	-
Gender (Male: Female)	52 : 18	55 : 15	0.3568	0.5503
UPDRS Off (Mean \pm SD)	NA	30.09 \pm 9.57	-	-
UPDRS On (Mean \pm SD)	NA	17.50 \pm 8.84	-	-
H&Y (Median)	NA	2	-	-
Age at Onset (Mean \pm SD)	NA	47.74 \pm 11.91	-	-

H & Y: Hoehn and Yahr scale; Pearson's chi-squared test for gender; SD: Standard Deviation; Student's T-test for age at onset; UPDRS: Unified Parkinson's Disease Rating Scale

B. Interregional grey matter correlations

The resulting association matrix for each of the groups contained 56 nodes (indicating to each ROI extracted, as in Appendix) and 1540 ($= 56*55/2$) of edges. Fig.1.A.1 and A.2 shows weighted undirected correlation matrix, Fig.1.B.1 and B.2 shows binary undirected correlation matrix and Fig.1.C.1 and C.2 shows Binary undirected networks of both HC and PD patient groups. The association matrices are mapped at minimum threshold (0.6 sparsity level) to obtain the binary undirected network in Fig.1 (C.1 and C.2). The binary undirected networks illustrate reduced number of edges in PD patients (Fig 1.C.1) compared to HC (Fig 1.C.2) at same level of sparsity. The strengths of the connections are indicated by the color-bar. The sparsity ranged between 0.6 to 0.9 with a step size of 0.03 for both groups. The average shortest path

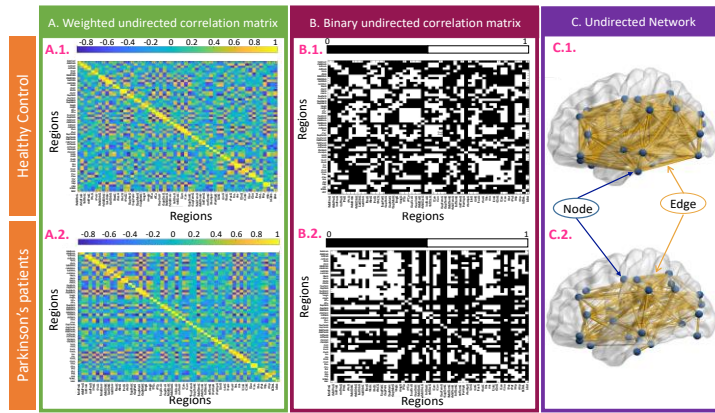


Figure 1. Weighted undirected Matrices, Binary undirected Matrices and Binary undirected networks of Healthy controls and Parkinson patients
Color-bar shows the strength of the connections.

length of the network under study was equivalent to that of the random network; the clustering coefficient of the network under study was greater than that of the random network; and the small-world index was larger than 1 over the sparsity range for either groups.

C. Network metrics and analysis

The distribution of mean clustering coefficient and mean local efficiency obtained from binary undirected correlation matrix are shown in Fig. 2 for PD patients and HC, along with the between-group differences. The results suggest that the mean clustering coefficient and mean local efficiency reduced with an increase in sparsity (Fig. 2. A.1 and B.1). The mean clustering coefficient of PD was found to be lesser than HC at a sparsity of 0.9 (Fig. 2. A.2), which signifies reduced local integration and disrupted communication in the disease. In line with our findings, clustering coefficient was observed to be lesser in early drug-naïve Parkinson patients in magnetoencephalography and diffusion tensor imaging studies respectively [15], [16]. The likelihood that a node's neighbors are related to one another is measured by its nodal clustering coefficient, and the average of nodal clustering coefficients of all nodes in a network is mean clustering coefficient. Previous study on PD with hemiparkinsonism and

HC showed no difference in clustering coefficient [9], while another investigation showed higher clustering coefficient in PD compared to HC [5]. Reduced local efficiency in PD at sparsities above 0.84 (Fig. 2. B.2) reveals restricted information exchangeability [7]. Nodal local efficiency assesses how efficient communication is among the node's immediate neighbors [9], [13], [17], when a node is removed. Similar to our results, impaired local efficiency was reported in PD from a longitudinal magnetoencephalographic study [15] and PD with tremor from a functional network study [7]. Additionally, PD patients with mild cognitive impairment were characterized with reduced local efficiency compared to PD with normal cognition and healthy controls, both [8]. On the contrary, PD patients were observed to have higher local efficiency from a morphological network analysis [7] and no difference from healthy control subjects in another study [9].

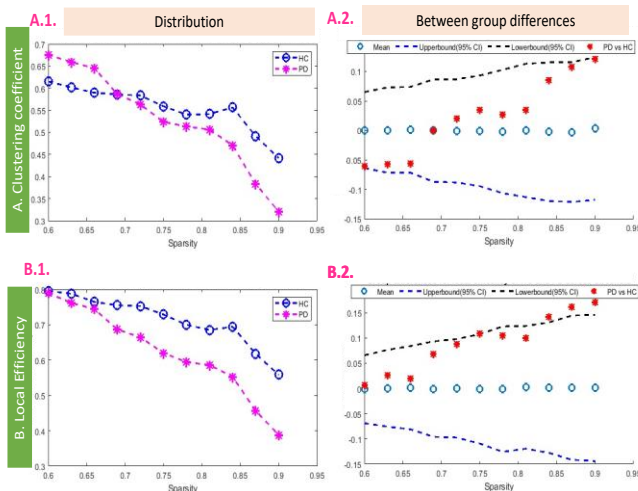


Figure 2. Distribution and intergroup differences in mean clustering coefficient and mean local efficiency

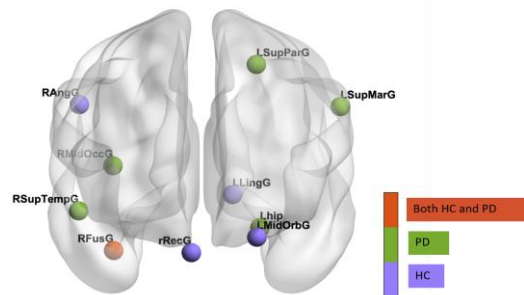


Figure 3. Hubs in healthy control (purple), PD (green) and common in both (red). Far regions appear to be in lighter shade.

Hubs are the important brain regions, playing key role in functional resilience, indicative of how brain regions interact to process information and effect responses. Hub regions were determined based on degree and betweenness centrality; higher degree indicated large number of connections to rest of the nodes in the network. The influence of a particular node on information flow between other nodes is described by a node's betweenness centrality [9], [13], [18]. The hub regions of HC (purple), PD (green) and common to both groups (red) are shown in Fig.3. Right fusiform gyrus was conserved in PD, while left middle orbitofrontal gyrus, right gyrus rectus,

right angular gyrus, left lingual gyrus were disrupted in PD and left superior parietal gyrus, left supramarginal gyrus, right middle occipital gyrus, right superior temporal gyrus, left hippocampus were regenerated in PD.

IV. CONCLUSION

Our connectivity analysis on sMRI-aided morphological network provided evidence of reduced clustering coefficient and reduced local efficiency. This represented disrupted network in PD and hence, could be used as a signature for distinguishing Parkinson's patients from healthy controls. Interestingly, so far in Parkinson's disease, our study presents a more concrete and statistically established results due to larger dataset.

There are limited studies on individual network analysis and it's challenging to design a brain network using cross-sectional sMRI data. Although prior multimodal research analysed brain connectivity independently, combining different features might provide additional information and new insights into network analysis. Brain connectivity analysis of subgroups of Parkinson's disease could be the way forward.

APPENDIX

Regions of LPBA atlas are below:

Abbreviations	Region Names
lSupFroG	L.superior.frontal.gyrus
rSupFroG	R.superior.frontal.gyrus
lMidFroG	L.middle.frontal.gyrus
rMidFroG	R.middle.frontal.gyrus
lInfFroG	L.inferior.frontal.gyrus
rInfFroG	R.inferior.frontal.gyrus
lPrcG	L.precentral.gyrus
rPrcG	R.precentral.gyrus
lMidOrbG	L.middle.orbitofrontal.gyrus
rMidOrbG	R.middle.orbitofrontal.gyrus
lLatOrbG	L.lateral.orbitofrontal.gyrus
rLatOrbG	R.lateral.orbitofrontal.gyrus
lRecG	L.gyrus.rectus
rRecG	R.gyrus.rectus
lPoCG	L.postcentral.gyrus
rPoCG	R.postcentral.gyrus
lSupParG	L.superior.parietal.gyrus
rSupParG	R.superior.parietal.gyrus
lSupMarG	L.supramarginal.gyrus
rSupMarG	R.supramarginal.gyrus
lAngG	L.angular.gyrus
rAngG	R.angular.gyrus
lPCu	L.precuneus
rPCu	R.precuneus
lSupOccG	L.superior.occipital.gyrus
rSupOccG	R.superior.occipital.gyrus
lMidOccG	L.middle.occipital.gyrus
rMidOccG	R.middle.occipital.gyrus
lInfOccG	L.inferior.occipital.gyrus
rInfOccG	R.inferior.occipital.gyrus
lCun	L.cuneus
rCun	R.cuneus
lSupTemG	L.superior.temporal.gyrus
rSupTemG	R.superior.temporal.gyrus
lMidTemG	L.middle.temporal.gyrus
rMidTemG	R.middle.temporal.gyrus
lInfTemG	L.inferior.temporal.gyrus
rInfTemG	R.inferior.temporal.gyrus
lParHipG	L.parahippocampal.gyrus
rParHipG	R.parahippocampal.gyrus
lLinG	L.lingual.gyrus

rLinG	R.lingual.gyrus
lFusG	L.fusiform.gyrus
rFusG	R.fusiform.gyrus
lIns	L.insular.cortex
rIns	R.insular.cortex
lCinG	L.cingulate.gyrus
rCinG	R.cingulate.gyrus
lCau	L.caudate
rCau	R.caudate
lPut	L.putamen
rPut	R.putamen
lHip	L.hippocampus
rHip	R.hippocampus
bCbEL	Cerebellum
bBst	Brainstem

REFERENCES

- [1] H. Braak, K. D. Tredici, U. Rüb, R. A. I. de Vos, E. N. H. Jansen Steur, and E. Braak, "Staging of brain pathology related to sporadic Parkinson's disease," *Neurobiology of Aging*, vol. 24(2), pp. 197–211, 2003.
- [2] T. Samantary, J. Saini, and C. N. Gupta, "Meta-Analysis of Clinical Symptoms and Data Driven Subtyping Approaches in Parkinson's Disease." The Brain Conference, 2021, Mar. 04, 2021. https://thebrainconference.co.uk/wp-content/uploads/2021/02/R2_51_Samantary_Tanmayee_MovementDisorders_51.png (Accessed last on 12th April 2022)
- [3] D. Berg *et al.*, "Time to redefine PD? Introductory statement of the MDS Task Force on the definition of Parkinson's disease," *Mov Disord*, vol. 29, no. 4, pp. 454–462, Apr. 2014.
- [4] X. Xu, Q. Han, J. Lin, L. Wang, F. Wu, and H. Shang, "Grey matter abnormalities in Parkinson's disease: a voxel-wise meta-analysis," *European Journal of Neurology*, vol. 27, no. 4, pp. 653–659, 2020.
- [5] Q. Wu, Y. Gao, A.-S. Liu, L.-Z. Xie, L. Qian, and X.-G. Yang, "Large-scale cortical volume correlation networks reveal disrupted small world patterns in Parkinson's disease," *Neuroscience Letters*, vol. 662, pp. 374–380, Jan. 2018.
- [6] S. K. Yadav *et al.*, "Gender-based analysis of cortical thickness and structural connectivity in Parkinson's disease," *J Neurol*, vol. 263, no. 11, pp. 2308–2318, Nov. 2016.
- [7] D. Zhang, J. Wang, X. Liu, J. Chen, and B. Liu, "Aberrant Brain Network Efficiency in Parkinson's Disease Patients with Tremor: A Multi-Modality Study," *Front. Aging Neurosci.*, vol. 7, Aug. 2015.
- [8] J. B. Pereira *et al.*, "Aberrant cerebral network topology and mild cognitive impairment in early Parkinson's disease: Aberrant Brain Network Topology in Early PD," *Hum. Brain Mapp.*, vol. 36(8), 2015.
- [9] X. Xu *et al.*, "Brain Atrophy and Reorganization of Structural Network in Parkinson's Disease With Hemiparkinsonism," *Frontiers in Human Neuroscience*, vol. 12, p. 117, 2018.
- [10] D. W. Shattuck *et al.*, "Construction of a 3D Probabilistic Atlas of Human Cortical Structures," *Neuroimage*, vol. 39(3), 1064–80, 2008.
- [11] A. Zalesky, A. Fornito, and E. Bullmore, "On the use of correlation as a measure of network connectivity," *Neuroimage*, vol. 60, no. 4, pp. 2096–2106, May 2012.
- [12] G. Sanabria-Diaz *et al.*, "Surface area and cortical thickness descriptors reveal different attributes of the structural human brain networks," *NeuroImage*, vol. 50, no. 4, pp. 1497–1510, May 2010.
- [13] M. Rubinov and O. Sporns, "Complex network measures of brain connectivity: Uses and interpretations," *NeuroImage*, vol. 52, no. 3, pp. 1059–1069, Sep. 2010.
- [14] M. Xia, J. Wang, and Y. He, "BrainNet Viewer: A Network Visualization Tool for Human Brain Connectomics," *PLoS ONE*, vol. 8, no. 7, Jul. 2013.
- [15] K. T. E. Olde Dubbelink *et al.*, "Disrupted brain network topology in Parkinson's disease: a longitudinal magnetoencephalography study," *Brain*, vol. 137, no. Pt 1, pp. 197–207, Jan. 2014.
- [16] S. Nigro *et al.*, "Characterizing structural neural networks in de novo Parkinson disease patients using diffusion tensor imaging," *Human Brain Mapping*, vol. 37, no. 12, pp. 4500–4510, 2016.
- [17] X. Liao, A. V. Vasilakos, and Y. He, "Small-world human brain networks: Perspectives and challenges," *Neuroscience & Biobehavioral Reviews*, vol. 77, pp. 286–300, Jun. 2017.
- [18] L. C. Freeman, "Centrality in social networks conceptual clarification," *Social Networks*, vol. 1, no. 3, pp. 215–239, Jan. 1978.